

Towards Efficient Large Multimodal Model Serving

Haoran Qiu¹ Anish Biswas¹ Zihan Zhao² Jayashree Mohan¹ Alind Khare¹ Esha Choukse¹
Íñigo Goiri¹ Zeyu Zhang² Haiying Shen² Chetan Bansal¹ Ramachandran Ramjee¹ Rodrigo Fonseca¹

¹Microsoft ²University of Virginia

Abstract

Recent advances in generative AI have led to large multimodal models (LMMs) capable of simultaneously processing inputs of various modalities such as text, images, video, and audio. While these models demonstrate impressive capabilities, efficiently serving them in production environments poses significant challenges due to their complex architectures and heterogeneous resource requirements.

We present the first comprehensive systems analysis of two prominent LMM architectures, decoder-only and cross-attention, on six representative open-source models. We investigate their multi-stage inference pipelines and resource utilization patterns that lead to unique systems design implications. We also present an in-depth analysis of production LMM inference traces, uncovering unique workload characteristics, including variable, heavy-tailed request distributions, diverse modal combinations, and bursty traffic patterns.

Our key findings reveal that different LMM inference stages exhibit highly heterogeneous performance characteristics and resource demands, while concurrent requests across modalities lead to significant performance interference. To address these challenges, we propose a decoupled serving architecture that enables independent resource allocation and adaptive scaling for each stage. We further propose optimizations such as stage colocation to maximize throughput and resource utilization while meeting the latency objectives.

1 Introduction

The rapid advancement in generative AI has led to the development of large multimodal models (LMMs) capable of processing inputs across various modalities such as text, image, video, and audio. These models have demonstrated remarkable capabilities in tasks like image captioning [5, 16, 34], visual question answering [44, 45], and multimodal dialogue systems [9, 22, 49]. This has led to their rapid adoption of LMMs in production services, including interactive applications where low latency is critical.

Unlike traditional large language models (LLMs) that process purely textual inputs using a single component, a decoder-based transformer architecture [52], LMMs handle fundamentally different types of inputs, each requiring distinct pro-

cessing approaches. This heterogeneity introduces unique serving complexities that demand novel analysis and serving strategies. For *Image-Text-to-Text* models [18]¹, the inference pipeline consists of multiple specialized stages: image preprocessing to transform raw images into tensor representations, image encoding to convert these tensors into image tokens, and a language model backend that combines text prompts with image tokens to generate textual outputs. Currently, these stages are typically served as a monolithic system [4, 20, 53], where all components are integrated within a single serving instance and scaled together as a unified entity.

In this paper, we present the first comprehensive systems analysis of two prominent LMM architectures, cross-attention (CA) and decoder-only (DO), by examining six representative open-source, *Image-Text-to-Text* models to understand their multi-stage inference pipelines and performance-resource characteristics. This analysis reveals unique systems design implications for production deployments. Additionally, through an in-depth study of production LMM traces, we uncover distinctive workload characteristics, including variable request patterns, diverse multi-modality combinations, and bursty traffic behaviors. While our study focuses on *Image-Text-to-Text* models rather than multimodal generation tasks like image or video synthesis [28], these models represent a significant and widely deployed class of LMMs that exemplify the fundamental challenges in multimodal serving.

Our systematic analysis reveals several key findings and their implications for LMM serving system design, as summarized in **Table 1**. First, CA models achieve an order of magnitude higher prefill efficiency compared to DO models with marginal accuracy tradeoffs, though each architecture exhibits unique performance characteristics that demand specialized optimization strategies. Second, the LMM inference workflow demonstrates significant heterogeneity, with stages showing distinct resource and performance patterns across batching, model sharding, and frequency scaling operations, necessitating decoupled execution. Third, image encoding emerges as a critical bottleneck, consuming a substantial portion of time-to-first-token (TTFT) across multiple models,

¹While our analysis centers on *Image-Text-to-Text* models, the insights and techniques we develop are applicable to other multimodal scenarios, including *Video-Text-to-Text* tasks where video can be processed as a sequence of image frames [23].

Table 1: Key findings and implications of our LMM characterization study.

<i>Findings</i>	<i>Implications</i>
Cross-attention models provide 10× higher prefill throughput than decoder-only ones albeit with small accuracy loss, but both show distinct performance patterns	Serving optimizations must be architecture specific
Each LMM stage exhibits distinct performance and resource characteristics regarding batching, model sharding, frequency scaling etc.	Decouple LMM stages and independently optimize the deployment of each stage
LMMs spend a significant part of their TTFT on image encoding	Parallelize and optimize image encoding to reduce TTFT
Heterogeneity in the composition of input modality results in interferences between text-only and image-text requests	Modality-aware scheduling to provide inter-request performance isolation
Production traffic shows heavy-tailed distributions with modality-specific bursts	Workload-aware autoscaling of the LMM stages

highlighting the need for parallelizing encoder computation to reduce latency. Fourth, mixing text-only and image-text requests introduces notable interference patterns that impact serving performance, necessitating modality-aware scheduling. Finally, our analysis of production workloads reveals heavy-tailed distributions with modality-specific bursts, underscoring the need for workload-aware autoscaling to cope with the dynamic nature of LMM serving requirements.

Our findings directly inform our proposed design of a novel *decoupled architecture* for efficient LMM serving (Section 6.1). This architecture treats the key pipeline stages—image preprocessing, image encoding, and language model operations such as prefill and decode—as independently scalable components. Our proposed design brings three key benefits and enables (1) fine-grained stage-aware resource management, (2) multimodal workload-specific scheduling/routing, and (3) model architecture-specific optimizations. We introduce stage-specific resource management policies that can be tailored to each stage’s unique characteristics. These policies encompass autoscaling, batching, and model sharding strategies, allowing the system to efficiently handle varying resource demands and optimize the latency-throughput tradeoff. This approach particularly allows for managing imbalanced modalities and diverse workloads with varying image counts and dimensions. We further propose (1) *stage colocation* (Section 6.4) to improve resource utilization by co-locating the compute-heavy image encoder and memory-bound language decoder, complementary to existing techniques like prefill-decode colocation in the context of LLMs [1, 20], and (2) *modality-aware scheduling* (Section 6.5), where the system adapts scheduling decisions based on workload composition and real-time resource availability.

Contributions. Our analysis reveals critical insights into the systems challenges of efficiently serving LMMs at scale, demonstrating how architectural choices and workload-aware optimizations can address these emerging challenges. This paper makes the following contributions:

- **Systematic LMM characterization:** We present a comprehensive analysis of LMM serving characteristics, examining performance profiles and resource utilization patterns across diverse workloads in both open-source LMM deployments and production environments.

- **Novel systems challenges:** We identify and analyze the unique challenges in serving LMM inference workloads, particularly highlighting how workload heterogeneity and request interference impact system design.
- **Decoupled serving architecture:** We propose a modular architecture for scalable LMM serving that enables fine-grained resource management, workload-aware scheduling, and model-specific optimizations.

2 Background

2.1 Large Multimodal Models

LMMs represent a significant evolution from text-centric LLMs by integrating capabilities to process and reason across multiple modalities, such as text and images in the Image-Text-to-Text category [18], enabling applications like visual question answering, image captioning, and other multimodal tasks. LMM architectures can be mainly categorized into two: (1) *decoder-only* LMMs, such as DeepSeek’s Janus Pro [7], LLaVA-OneVision [23], InternVL [9], and NVLM-D [12]; and (2) *cross-attention-based* LMMs, such as Llama-3.2 Vision [11], NVLM-X [12], and Flamingo [2]. While the two types of architectures have common image preprocessing and image encoding stages (see Figure 1), they differ in how the image tokens are processed in the language model backend.

Image Preprocessing. Image preprocessing and encoding are the first steps to convert raw image inputs to image tokens before feeding them to the language model backend. While LMM architecture continues to evolve, image preprocessing methods become increasingly standardized regardless of the underlying architectural choices. Typically, LMMs follow four key processing steps: (1) transform the raw image with resizing, rescaling, padding, and normalization, (2) segment the transformed image into tiles [9, 11, 12] or patches [23], (3) apply additional tile/patch-level transformations, and (4) incorporate a thumbnail with the rest of image tiles.

Despite the similarities discussed above, the number of tiles or patches generated by different image processors can differ significantly, leading to distinct relationships between image dimensions and image tokens. For instance, NVLM-D restricts the number of tiles per image to a maximum of 6

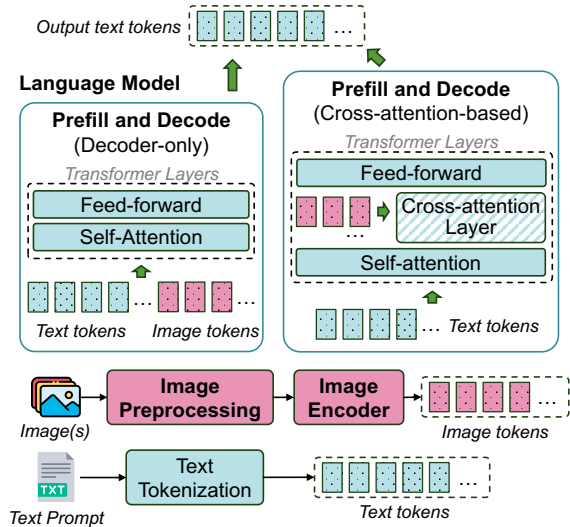


Figure 1: Model architecture for decoder-only and cross-attention-based LMMs.

tiles, with one additional thumbnail tile [12], while InternVL allows a maximum of 12 tiles per image plus a thumbnail tile [9]. Llama-3.2 Vision also adopts a similar strategy by setting a maximum of 4 tiles for each image [11]. In contrast, LLaVA-OneVision has a loose restriction, supporting up to 36 tiles for a high-resolution image with an additional thumbnail tile [23], leading to a much higher number of generated image tokens than the other models. For instance, in Table 2, an 896×896 image can have 4, 5, and 10 tiles of various sizes in six representative open-source LMMs.

Image Encoding. The image encoder takes processed image tiles as input and produces image tokens that are then passed to the language model backend. Today’s image encoders predominantly use the vision transformer architecture [3] to extract visual features from images, with different models adopting variations tailored to their specific requirements. For example, LLaVA-OneVision uses SigLIP [55], InternVL and NVLM-D use InternViT [9], and Llama-3.2 Vision uses ViT-H [3]. In LLaVA-OneVision, the image encoder is limited to generate a maximum of 729 tokens per tile for single-image inputs [23]. In contrast, InternVL and NVLM-D restrict this to a fixed number of 256 tokens per tile [9, 12], while Llama-3.2 Vision sets the number at 1601 tokens per tile [11]. Therefore, in the example of an 896×896 image (Table 2), the total number of image tokens generated from the image encoders ranges from 1280 to 7290 across different open-source LMMs.

Decoder-Only (DO) LMMs. A DO LMM reuses an existing LLM backend with no changes, with text and image tokens homogeneously flowing through the LLM backend (as shown in the “decoder-only” box in Figure 1). DO architectures are favored for their simplicity and unified handling

of all modalities as input sequences; however, they often require substantial sequence lengths for high-resolution image processing, leading to computational inefficiencies.

Cross-Attention (CA)-based LMMs. In contrast to DO LMMs that make no architectural changes to the language model backend, CA-based models like Llama-3.2 Vision and NVLM-X insert *cross-attention layers* into the language model to process flattened image tokens, akin to treating visual inputs as a “foreign language” in an encoder-decoder transformer setup. While more complex to train, CA-based models excel in inference-time computational efficiency, as they avoid unrolling all image tokens in the LLM decoder, making them well-suited for high-resolution inputs. As shown in the “cross-attention” box of Figure 1, the self-attention layer’s input only includes text tokens, while the CA layer attends to both the text tokens and the image tokens.

2.2 Monolithic LMM Deployment

LMMs are typically implemented as *monolithic* systems in current serving frameworks [20, 53]. This means that all inference components (image preprocessor, image encoder, and language model backend) are deployed as an ensemble, reside in the same model instance, and are thus co-located on the same hardware node. These components operate in a tightly coupled manner, with uniform batching and model parallelism strategies applied across the entire pipeline. This monolithic approach is straightforward to implement and widely used in open-source platforms for Image-Text-to-Text tasks.

Model Parallelism. It is widely accepted that the model parallelism strategy for LLM inference should depend on memory capacity for the request batch size and prompt length to serve. Tensor parallelism (TP) is used to split the model along the attention head dimension on multiple GPUs inside each node. Pipeline parallelism (PP) is used to split the model along the model layer dimension on multiple nodes [50]. The same has been extended for LMMs so far, with both encoder and LLM following the same parallelism strategy [20]. The default model parallelism in our characterization study on open-source LMMs is listed in Table 2.

2.3 SLO Metrics for LMM Inference

Two major SLO metrics are commonly used for production LLM/LMM model serving systems, with a focus on tail latency to ensure SLOs reflect the worst-case performance for end-user satisfaction:

- **Time to First Token (TTFT):** This measures the latency from a user query, including text and/or image(s), to the generation of the first token in the response. It reflects the responsiveness of the model, which is essential for interactive applications such as real-time question-answering and dialog systems. Note that compared to text-only LLMs, LMM-serving’s TTFT to a request comprises (1) image

Table 2: Models and encoder configurations for a 896×896 input image. All the models use a patch size of 14×14 .

LMM Model Name	Abbreviation	Architecture	Tile Size	Image Encoder (#Params)	Total Image Token Size (#Tiles \times #Tokens \times DSR)	LLM Backend (#Params)	Tensor Parallelism	Average Accuracy (HF-VLM [14])
Llama 3.2 Vision 11B [30]	Llama3.2-11B	Cross-attention	560 \times 560	ViT-H/14 (630M)	$4 \times 1601 \times 1 = 6404$	Llama 3.1 (8B)	TP-4	57.8%
Llama 3.2 Vision 90B [31]	Llama3.2-90B	Cross-attention	560 \times 560	ViT-H/14 (630M)	$4 \times 1601 \times 1 = 6404$	Llama 3.1 (70B)	TP-8	63.4%
LLaVA-OneVision 7B [26]	LLaVA-OV-7B	Decoder-only	384 \times 384	SigLIP (400M)	$10 \times 729 \times 1 = 7290$	Qwen2 (7B)	TP-4	60.1%
LLaVA-OneVision 72B [25]	LLaVA-OV-72B	Decoder-only	384 \times 384	SigLIP (400M)	$10 \times 729 \times 1 = 7290$	Qwen2 (72B)	TP-8	68%
InternVL-2.5 26B [10]	InternVL-26B	Decoder-only	448 \times 448	InternViT (6B)	$5 \times 1024 \times 0.25 = 1280$	InternLM (20B)	TP-8	71.6%
NVLM-D 72B [13]	NVLM-D-72B	Decoder-only	448 \times 448	InternViT (6B)	$5 \times 1024 \times 0.25 = 1280$	Qwen2-Instruct (72B)	TP-8	67.6%

preprocessing time, (2) image encoding latency, and (3) language model prefill time.

- **Time Between Tokens (TBT):** This quantifies the delay between consecutive token generations during the decoding phase on the language model backend, directly impacting the perceived fluency and coherence of the model’s output. While meeting TTFT/TBT SLOs, an ideal LMM-serving system should maximize its request-serving *throughput* and compute resource *utilization*. Together, these metrics provide a balanced view of individual query responsiveness and system-wide efficiency, guiding the design and optimization of LMM serving frameworks.

3 Characterization on Open-Source LMMs

We characterize representative open-source LMMs (in the *Image-Text-to-Text* category [18]) on open-source datasets to evaluate the performance, resource requirements, and energy efficiency of all inference stages involved under varying input complexities and resource management configurations.

3.1 Experimental Setup

Hardware. We run the experiments on two setups: a DGX-A100 server with 8 NVIDIA A100 GPUs [33] and a DGX-H100 server with 8 NVIDIA H100 GPUs [32]. Each GPU has 80GB of high-bandwidth memory, and each server has NVLINK across GPUs. The CPU processor on the A100 node has 96 physical 2nd-generation AMD Epyc™ 7V12 (Rome) CPU cores, while the CPU processor on the H100 node has 96 physical Intel Xeon (Sapphire Rapids) cores. Both nodes have 1900 GiB DRAM memory. Unless specified, the experiments presented in this section are performed on the A100 node.

Models. We use six open-source models across two different LMM architectures, including CA-based models: Llama 3.2 Vision (11B and 90B) [11], and DO models: LLaVA-OneVision (7B and 72B) [23], InternVL-2.5 (26B) [9], and NVLM-D (72B) [12]. The details of the image encoder and LLM backend used by these models are listed in Table 2. The selected LMMs represent different model architectures (CA and DO), image encoder sizes (400M to 6B), and language model sizes (7B to 72B). We deploy the models on

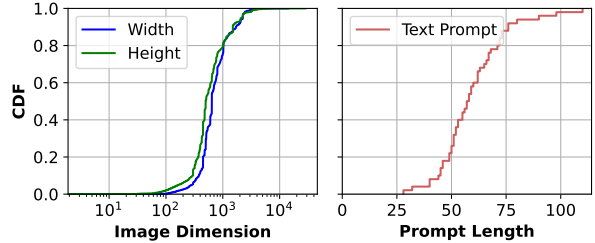


Figure 2: Image dimension distribution and text prompt length distribution of ShareGPT-4o Image dataset [8].

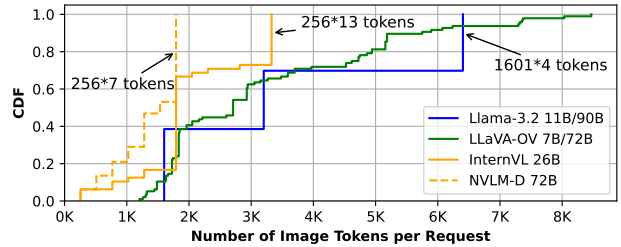


Figure 3: Distribution of image token count (per request) for open-source LMMs. Note that different models (e.g., LLaVA-OV 7B and 72B) can share the same image encoder so the number of image tokens are the same.

vLLM [20] in BF16, where the encoder and the LLM share the same tensor parallel degree (as described in Section 2.2).

Dataset. We use the open-source ShareGPT-4o LMM dataset [8] for image and text input. This dataset contains 50K images of varying resolutions and text prompt distributions (from GPT-4o) as shown in Figure 2.

Image Tokens Post Encoding. Figure 3 visualizes the distribution of image tokens generated per image when running the image encoders on the ShareGPT-4o dataset. We observe that the number of image tokens varies significantly across models. For instance, Llama3.2-11B/90B generates 2 to 4 tiles for each image in the ShareGPT dataset, and each tile results in 1601 tokens. The distribution for LLaVA-OV 7B/72B’s image encoder is more spread out, indicating a wider range of image token counts per request (with a min of 1205 tokens and a max of 8468 tokens). NVLM-D 72B and InternVL 26B

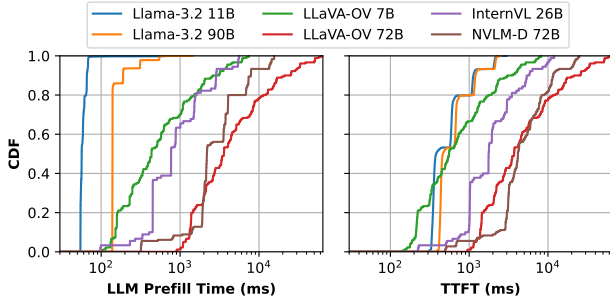


Figure 4: Distribution of TTFT and language model prefill times across open-source LMMs on the ShareGPT-4o dataset.

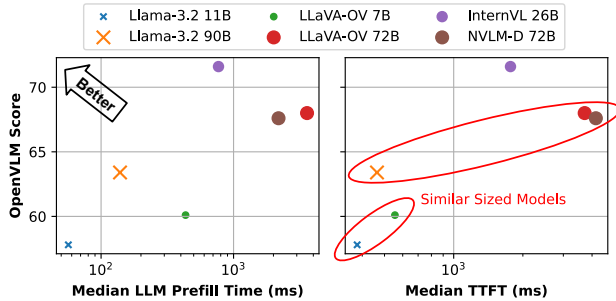


Figure 5: LMM accuracy vs. prefill/TTFT efficiency.

exhibit a similar spread-out pattern but with a lower min of 256 tokens and a lower max of 256×7 and 256×13 tokens on the ShareGPT-4o image dataset, respectively. Note that irrespective of the model, the text input per request is comparatively low, with a median of 57 and a maximum of 120 tokens for the ShareGPT-4o dataset as shown in Figure 2.

3.2 Comparing Different LMM Architectures

We now present a detailed characterization study of open-source LMMs and highlight the key takeaways.

Latency. Figure 4 plots the CDF of TTFT and language model prefill time of all the models on the ShareGPT-4o dataset. Comparing models with similar language model backend sizes across the two architectures (*i.e.*, Llama3.2-11B vs. LLaVA-OV-7B, and Llama3.2-90B vs. LLaVA-OV-72B vs. NVLM-D-72B), we observe that CA-based counterparts have up to an order of magnitude lower LLM prefill execution time compared to DO models, and thus lower TTFT. This is because, given the same amount of image tokens and text tokens, DO models feed all tokens in the self-attention layers of the language model backend, while CA models only feed text tokens in the self-attention layers.

Accuracy. Figure 5 plots the accuracy vs. prefill/TTFT efficiency of different models. Comparing models of similar size across the two architectures, the CA counterparts are typically

5 points lower in accuracy compared to the DO models on the Open VLM leaderboard [14]; *e.g.*, Llama3.2-90B gets a score of 63.4, while a similarly sized LLaVA-OV-72B gets 68 points but at an order of magnitude higher prefill latency. CA models could close the accuracy gap by using a larger LLM backbone without substantially increasing prefill latency. For instance, Llama3.2-90B achieves about 6 points higher than Llama3.2-11B at a marginal 22% increase in TTFT.

Finding 1: CA models achieve an order of magnitude lower prefill latency at the cost of being a few points less accurate than similar-sized DO models, resulting in a better efficiency-to-accuracy ratio.

3.3 LMM Per-stage Breakdown Analysis

Figure 6 plots the split-up of TTFT across the three stages that comprise it: image preprocessing, image encoding, and LLM prefill. There are three key takeaways. First, image preprocessing, which occurs on the CPU, contributes minimally to the overall TTFT, while image encoding time contributes to a major portion of TTFT (especially for CA models). For instance, 79% and 65% of TTFT in Llama3.2-11B and Llama3.2-90B are from image encoding. For DO models such as InternVL-26B and NVLM-D-72B, image encoding latency accounts for 25% and 54% of TTFT. Second, the image encoding time depends on the encoder model size. For instance, scaling from SigLIP-400M (in LLaVA-OV-7B) to InternViT-6B (in InternVL-26B), the median image encoding time increases by 10x. Finally, prefill computation is more efficient in CA models because image tokens are attended to only in the CA layers, as previously discussed in Section 3.2.

Finding 2: The majority of time-to-first-token (TTFT) is spent on image encoding in CA models due to higher prefill efficiency by introducing CA layers.

Compute Characteristics of LMM Stages. Image preprocessing on CPU and image encoding on GPU are compute-intensive processes. Figure 7a plots the impact of varying the number of CPU cores on preprocessing latency. It is evident that preprocessing is CPU-intensive, and benefits from trivially parallelizing across all the available cores. Both stages exhibit linear latency scaling with batch size, saturating compute without significant throughput gains from increased batching as shown in Figures 7b and 7c, respectively.

Figure 7d further plots the GPU utilization metrics for a request batch size of one during image preprocessing and image encoding. We observe a consistent SM core activity near 100% during image encoding, with average DRAM utilization below 30%. Image encoding is, therefore, typically compute-bound, resembling the language model’s prefill phase [19]. We do not investigate the compute characteristics of prefill

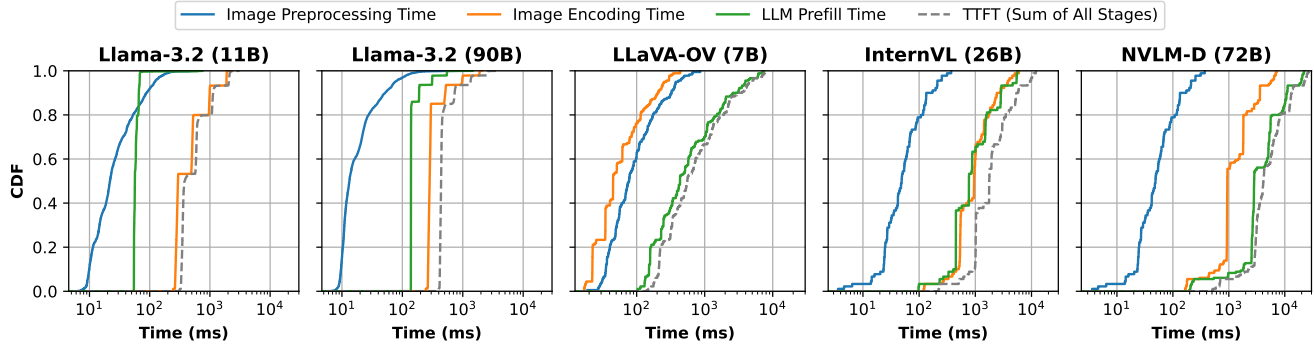


Figure 6: Per-stage request latency breakdown analysis across representative open-source LLMs deployed using default TP parallelism. Note that TTFT (dashed line) is the sum of the latency from each stage (i.e., TTFT = image preprocessing time + image encoding time + language model prefill time).

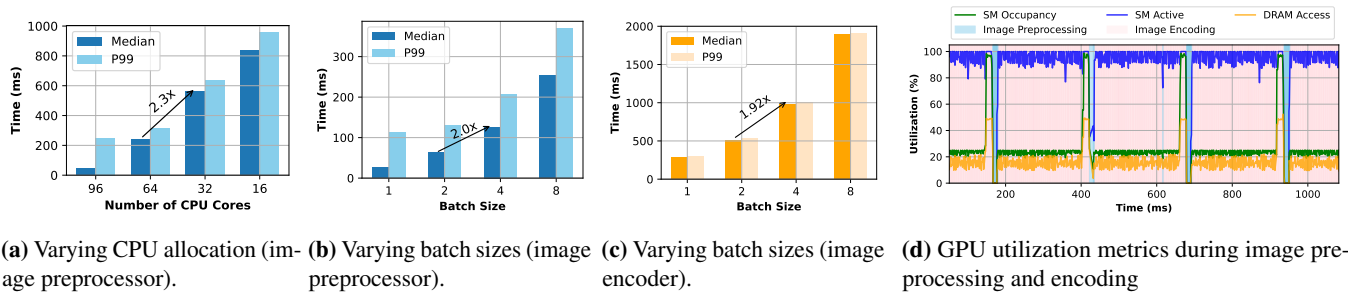


Figure 7: Compute characteristics of image preprocessing and encoding. Both the stages are compute-bound.

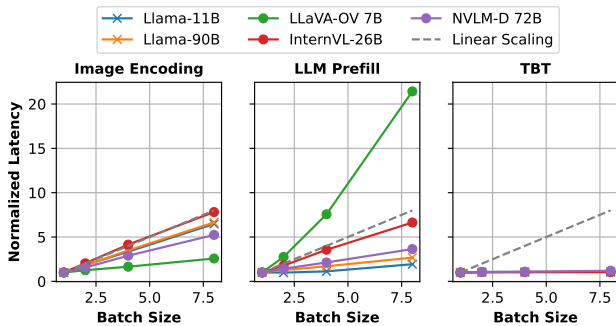


Figure 8: Median latency vs. batch size per LLM stage on GPUs. Latency is normalized to that at batch size one.

and decode phases of the language model as it has been well studied; the prefill phase is typically compute-bound, while the decode phase is memory-bound [1, 19, 40].

Finding 3: Image preprocessing (on CPU) and encoding (on GPU) are both compute-intensive stages similar to LLM prefill computation.

Impact of Homogeneous Batching Across Stages on GPU. In today’s monolithic deployments, a single batch size is applied across all stages of the LLM on the GPU, which does not strike a balance between latency and throughput. To illustrate this, we plot Figure 8 that shows the impact of the

batch size on the median latency of every LLM stage across different model architectures. As the batch size increases, the increase in the median latency for different LLM stages increases at different rates. This variation highlights the diverse sensitivity of each LLM stage to batch size, and their varying levels of compute-intensiveness.

Compute-intensive stages like image encoding and LLM prefill (in DO models) show minimal throughput gains and increased latency beyond small batch sizes. In contrast, the memory-bound decode stage exhibits linear throughput improvement with increasing batch size. Notably, for this multimodal dataset’s low text token count, CA models uniquely benefit from prefill batching, diverging from traditional LLM literature which suggests prefills saturate compute even at a batch size of one single request. Therefore, request batching strategies should be tailored to each stage of the model based on its computational characteristics.

Finding 4: The effectiveness of batching for image encoding and language model’s prefill/decode varies and is model-specific. Image encoding benefits the least from batching, except for LLaVA-OV-7B.

Impact of Parallelism. Figure 9 shows the latency trend of each stage when independently increasing TP degrees of each LLM component. In Llama3.2-11B, the lowest LLM prefill time is achieved at TP-8, while the lowest image encoding la-

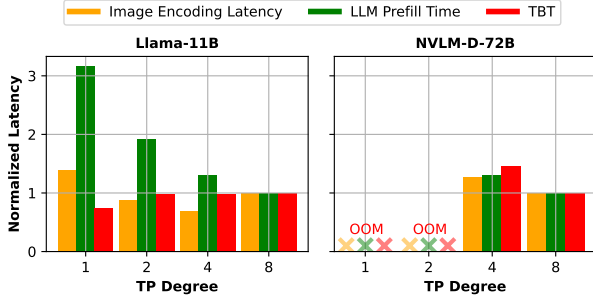


Figure 9: Impact of the tensor parallelism (TP) degree on the median latency of each stage for CA-based and DO LMMs. Latency is normalized to that of TP-8.

tency is at TP-4 and the lowest TBT at TP-1. In fact, encoding latency increases at TP-8 because TP performance trends are influenced by tradeoffs in compute intensity and inter-GPU communication overhead, making it inefficient to split a small 630M encoder across 8 GPUs.

Alternately, in NVLM-D-72B, which features a significantly larger image encoder (6B compared to 630M), the image encoding latency is reduced by $1.3\times$ when increasing the TP degree from 4 to 8. However, this results in diminishing returns relative to the increased resource cost. Depending on the workload traffic and application requirements (whether higher throughput or lower latency is needed), operators can choose between deploying two image encoders with TP-4 (to maximize throughput) or one encoder with TP-8 (to minimize latency), both across 8 GPUs.

These results highlight that treating the image encoder and LLM backend as a monolithic unit when determining parallelism strategies can lead to suboptimal performance. Instead, deployment decisions should account for their individual architectural characteristics and computation intensity to achieve optimal efficiency.

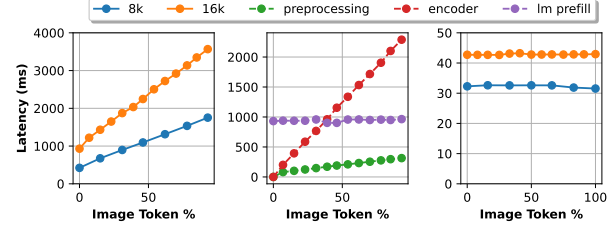
Finding 5: Image encoder and LLM backend can scale differently with model parallelism, while a monolith deployment limits the sharding flexibility and results in suboptimal performance.

3.4 Mixed Modality Performance Variation

Image-Text-to-Text LMMs handle a mixed workload, processing both text-only and image-text requests simultaneously, as not all requests include an image input. In this section, we explore the effects of mixing images with text prompts on both an *intra-request* and *inter-request* level.

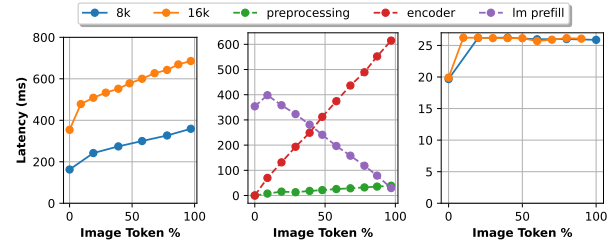
3.4.1 Impact of Intra-Request Image-Text Token Ratio

Figure 10 shows how varying image-to-text token ratios within a single request affects TTFT, with corresponding



(i). Average TTFT. (ii). TTFT breakdown. (iii). Average TBT.

(a) InternVL-26B



(i). Average TTFT. (ii). TTFT breakdown. (iii). Average TBT.

(b) Llama3.2-11B

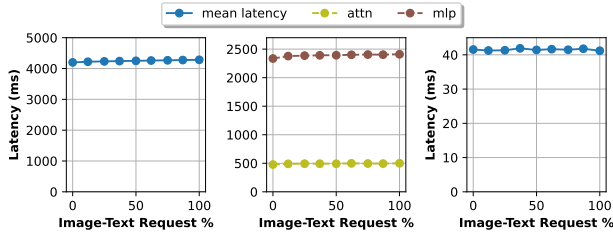
Figure 10: Request TTFT/TBT and time breakdown for a context length of 16K under various image-to-text token ratios for InternVL-26B (DO) and Llama3.2-11B (CA).

component-wise latency breakdowns. We fix the total context length of each request at 8K and 16K tokens while varying the percentage of image tokens by adjusting the number of images (0–12 images for InternVL-26B with 1280 tokens/image, 0–10 for Llama3.2-11B with 1601 tokens/image).

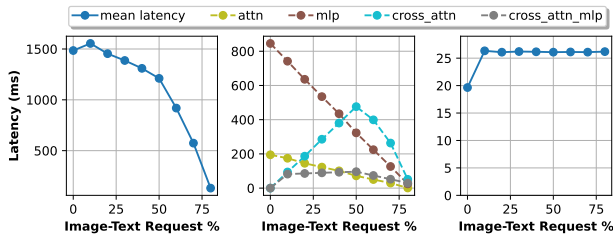
For the DO InternVL-26B model, TTFT increases linearly with image token percentage, primarily driven by image encoding time, while prefill latency remains constant as shown by the split in Figure 10a (ii). This stability in prefill latency stems from decoder-only LMMs processing both text and image tokens similarly through the language model backend. Notably, increasing from 1 to 12 images results in $10\times$ higher encoder latency, leading to $3\times$ higher TTFT.

The CA-based Llama3.2-11B model shows a different pattern. While TTFT increases with image token percentage due to encoder overhead, the impact is less severe than InternVL-26B, showing only $1.5\times$ TTFT degradation when moving from text-only to image-only inputs. This moderate latency gain is due to CA models attending to image tokens only in the CA layers, resulting in lower self-attention compute as the percentage of image tokens increases as shown in Figure 10b(ii). This partially offsets the increased image encoding latency.

The TBT behavior also differs between architectures. InternVL-26B’s TBT (batch size 64) remains stable as the image-text token split has no impact on DO models; compute is driven by the total context length. In contrast, Llama3.2-11B’s TBT (batch size 16) jumps sharply with the first image due to the activation of the CA layers and then stabilizes as



(i). Prefill latency. (ii). Prefill breakdown. (iii). Average TBT.
(a) InternVL-26B.



(i). Prefill latency. (ii). Prefill breakdown. (iii). Average TBT.
(b) Llama3.2-11B.

Figure 11: LLM prefill time and TBT under various image-text request ratios in a mixed batch of requests for InternVL-26B (DO) and Llama3.2-11B (CA).

image key-value vectors are cached during prefill.

Finding 6: As image tokens in a multimodal request increase, we see a more pronounced linear increase in TTFT for DO models due to encoder overhead.

3.4.2 Impact of Inter-Request Image-Text Request Ratio

We now evaluate the impact of inter-request batching of text-only and image-text requests on their latency to identify how they interfere with one another during the shared language model prefill and decode operations. Using a fixed batch size of 8 and a total context length of 64K tokens for both Llama3.2-11B and InternVL-26B, we vary the proportion of image-text requests in a batch from 0% (all text-only requests) to 100% (all image-text requests) and measure their prefill latency and TBT. The results are shown in Figure 11. Note that image encoding time increases at a higher rate than prefill latency as the image-text request ratio increases, but we focus on the trends in prefill execution time as the encoder latency can be reduced by independently scaling it.

For CA-based Llama3.2-11B, if a batch of text-only requests is batched with even a single image-text request, it would increase the average prefill latency and TBT of the text-only requests by 5.7% and 33.3% respectively, due to the activation of CA layers. However, as the image-text request ratio increases to 100%, prefill latency drops by 91% as reduced self-attention and its MLP computation outweigh the

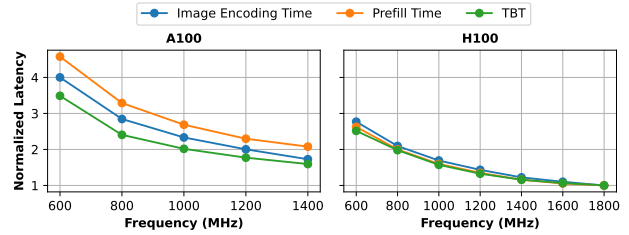


Figure 12: Performance impact on different stages under GPU frequency scaling on A100 and H100 nodes. Latency is normalized to that on H100 at 1800 MHz.

CA overhead. TBT, on the other hand, very slightly decreases as we increase the number of image-text requests beyond one because of the reduction in self-attention latency due to reduced KV accesses of the text tokens. The effect will be more pronounced at larger decode batches.

In contrast to the CA model, the DO InternVL-26B model shows negligible variance in TTFT and TBT as we vary the percentage of image-text requests in a batch. This is primarily due to the fact that both prefill and decode compute depend only on the total context length or batch size, as the DO models treat text and image tokens equally.

Finding 7: Batching requests of different modalities (image-text and text-only) results in performance variation and interference in the more efficient CA models.

3.5 Hardware and Power Sensitivity

To evaluate the sensitivity of hardware and power efficiency across LMM inference stages, we conducted a series of experiments on NVIDIA A100 and H100 GPUs to measure critical performance metrics, including image encoding latency, prefill time, and TBT, as well as GPU power consumption, under varying GPU frequency settings. All experiments presented in the rest of this section use Llama3.2-11B because CA-based LMMs achieve superior prefill efficiency and better overall TTFT and TBT than DO LMMs. Power consumption is measured using NVIDIA DCGM [36].

Performance. Figure 12 illustrates the impact of frequency scaling on performance across different inference stages at a batch size of eight. Similar trends are observed for other batch sizes. Image encoding latency improved by an average of 34% on A100 GPUs and 36% on H100 GPUs when scaling from the lowest to the highest frequency. Prefill times exhibited similar improvements, with an average gain of 30% on A100 and 28.5% on H100 GPUs. TBT, which represents the overall decoding performance, shows the least performance improvements of 17.3% on A100 and 14.1% on H100 due to its more memory-bound nature.

Transitioning from A100 to H100 hardware provided additional performance boosts. For image encoding latency, the

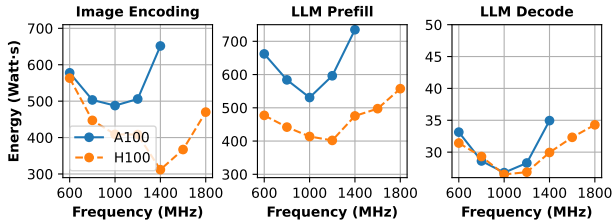


Figure 13: Impact of frequency scaling on the power consumption and performance on A100 and H100 nodes.

average improvement across all frequency levels is 30.4%. Prefill times improve by an average of 41.6%, with the highest gains for the lowest frequency level (44.2% at 1400 MHz). For TBT, the average improvement across frequency levels is only 23%, which is smaller than that in both image encoding and prefill. These results highlight the combined effects of frequency scaling and hardware upgrades on overall performance for both image encoding and language model prefill/decode workloads at varying batch sizes.

Finding 8: Image encoding has a higher performance degradation when downscaling GPU frequency compared to LLM prefill/decode.

Energy Efficiency. At higher frequencies, performance improvements come at the cost of increased power consumption. For example, when serving a batch of eight requests on an A100 device, peak power usage rises to 418 Watts during image encoding, 438 Watts during language model prefill, and 309 Watts during decoding.

Figure 13 shows energy consumption (power over execution time) across different frequencies for each LMM stage. Optimizing frequency requires balancing performance gains against diminishing returns in energy efficiency. This trend remains consistent across all stages (*i.e.*, image encoding, LLM prefill, and LLM decode) and different batch sizes.

The frequency setting that minimizes energy consumption (measured in *Watt-s*) varies by stage and GPU model. For image encoding, the optimal frequency is 1400 MHz on H100 and 1000 MHz on A100. For LLM prefill, it is 1200 MHz on H100 and 1000 MHz on A100, while for LLM decode, the optimal frequency is 1000 MHz on both GPUs.

At the optimal energy efficiency point, H100 GPUs consume 36% less energy than A100 GPUs during image encoding and 24% less during LLM prefill for a batch size of 8. However, for LLM decode, the difference in energy efficiency between H100 and A100 is only 1%.

Finding 9: Image encoding and LLM prefill benefit more from a higher-end GPU like H100, which achieves better energy efficiency, while LLM decode does not.

4 Production Trace Analysis

To understand multimodal serving patterns at scale, we analyze production traces from one of Azure’s LMM inference clusters. With LMMs becoming critical components in production services, we focus on characterizing the multi-tenant traffic consisting of both text-only and image-text requests. Our analysis specifically examines (1) temporal patterns and burstiness in workload characteristics and (2) statistical distributions of multimodal request patterns. We will be releasing the traces discussed soon.

Bursty and Variable Request Arrival Pattern. Our analysis, shown in Figure 14, examines (1) the traffic of text-only and image-text requests separately to understand their dynamic behavior and overall impact on the system, and (2) the traces of two different categories of services, image-heavy and text-heavy, to capture the diverse dynamics prevalent in production. The traces are collected over a span of two days. To understand the traffic patterns, we report the timeline of: (1) prompt (input) token rate, (2) output token rate, (3) request arrival rate, and (4) input image rate. Our analysis reveals two key characteristics of production traffic:

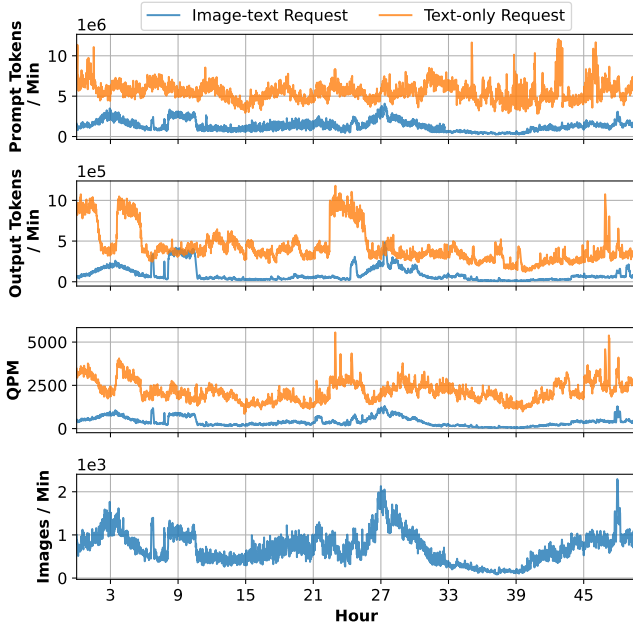
- **Diverse Request Arrival Patterns.** For image-heavy services, image-text requests show up to 5× higher prompt token rates compared to text-only requests, while text-heavy services demonstrate the opposite trend, with text-only requests having 3× higher rates. In addition, text-only and image-text request workloads often exhibit independently occurring peaks and troughs, showing minimal correlation.
- **Image Bursts.** Image-text request prompt token rates show bursty behavior across both service categories. In image-heavy services, these bursts arise from increased images per request rather than higher request arrival rates.

Heterogeneous Request Inputs. Given the significant variability in prompt token rates, we analyze input heterogeneity by examining prompt length distributions for both text-only and image-text requests (Figure 15a). The takeaways are:

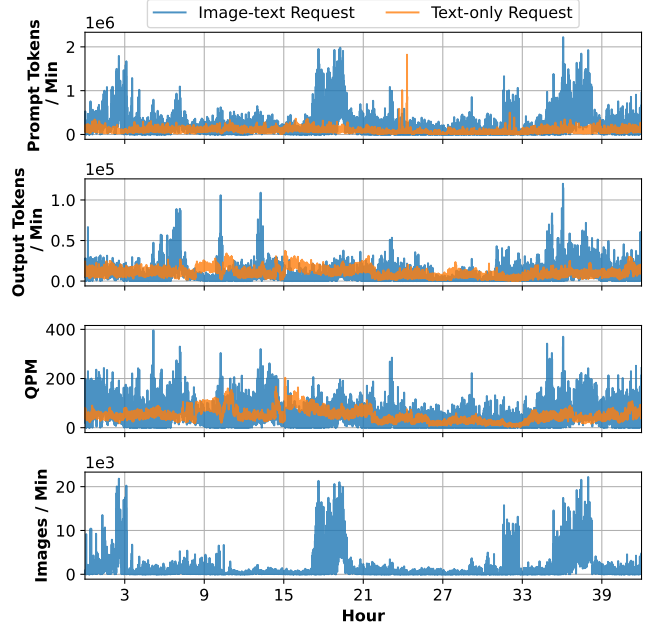
- **Heavy Tails in Prompt Lengths.** The services have heavy-tailed prompt length distribution. Both image-text and text-only requests’ prompt length distribution is a power-law² with alpha of 4.4 and 2.9, respectively.
- **Distinct Characteristics of Image-Text and Text-only Requests.** The image-text requests (solid line in Figure 15a) have longer median prompt lengths but shorter tail prompt lengths compared to text-only requests (dashed line).

We also assess how images contribute to the bursts in the prompt token rates. Images can lead to higher prompt length in two ways in LMMs: (1) More number of images per request, and thus more image tokens, and (2) higher dimension (resolution), and thus more tiles. To understand image bursts prevalent in production traces, Figures 15b and 16 show the

²In a power law distribution, a lower alpha value signifies a heavier tail with more extreme events occurring more frequently.

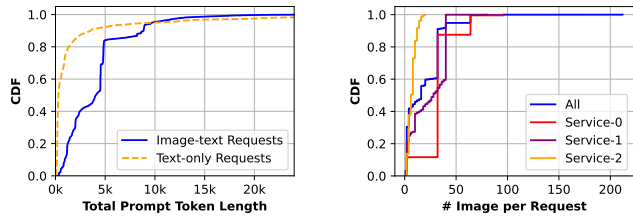


(a) Text-heavy services.



(b) Image-heavy services.

Figure 14: Aggregated Prompt token rate, token generation rate, request arrival rates in Queries per Minute (QPM), and image rate for a production LMM inference cluster in a two-day period for text and image heavy services.



(a) Total prompt length distribution in text-heavy services.

(b) Distribution of images per request in text-heavy services.

Figure 15: LMM input characterization in production.

distribution of the number of images per request and image dimensions, respectively, for the top 3 text-heavy services with the highest load. We examine both intra-service and inter-service image heterogeneity by comparing image input patterns within individual services and across different ones. This analysis helps determine whether image variability is primarily a service-specific characteristic or varies significantly across different services. The main takeaways are:

- **Inter-Service Heterogeneity in Images.** The input images exhibit a high inter-service heterogeneity in the number of images per request and image dimensions: (1) The P95 of the number of images per request for services 1 and 2 is 64 and order-magnitude higher than service 3 which is 4 (*i.e.*, a 16 \times factor difference as shown in Figure 15b). (2) Image dimensions also vary significantly between the services.

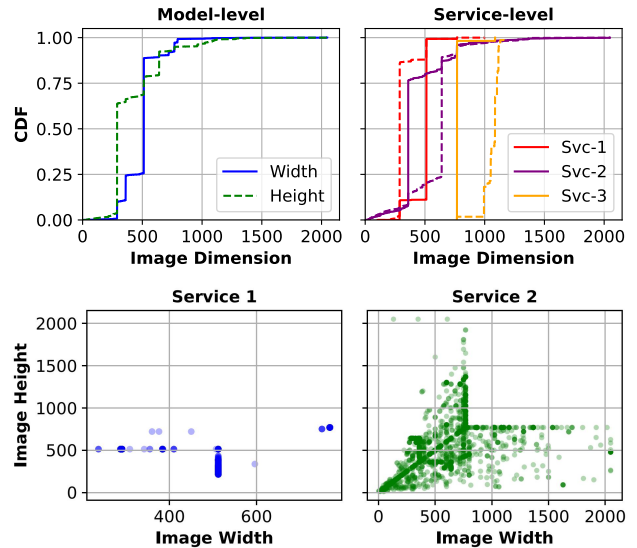


Figure 16: Image dimension distribution in production.

The P95 image height and width of Service 2 is 768×1117 , higher than the image dimensions of service 3, which is 512×512 (as shown in Figure 16 top row).

- **Heavy Tails in Images Per Request.** The number of images per request varies significantly and follows a power law distribution with alpha 1.5 (blue line in Figure 15b).

Finding 10: Production LMM traffic exhibits heavy-tailed distributions with modality-specific bursts, where image and text requests show independent peaks and variability in arrival patterns.

Comparison to ShareGPT-4o Dataset. We compare our production traces with the ShareGPT-4o LMM dataset [8]. Image dimensions show similar distributions across both datasets, with median width and height around 500 pixels and P95 exceeding 1000 pixels. However, text prompt lengths in the ShareGPT-4o dataset are 5× shorter, with a median length of 57 compared to 296 in production traces. The text accompanying images is also significantly shorter than the average text prompt length in LLMs found in popular open-source datasets like ShareGPT text dataset [51].

Finding 11: Open-source LMM inference datasets share similar image dimensions with production traces but have much shorter text prompts, common in visual question answering.

5 Challenges and Systems Implications

Based on our systems characterization study of open-source LMM benchmarks and production LMM workloads, we discuss the key challenges and their implications for designing efficient LMM serving at scale.

5.1 Implications on Systems Architecture

Our characterization analysis (Section 3) on diverse, representative open-source LMM models for Image-Text-to-Text tasks reveals the following key aspects that significantly impact the design of efficient LMM serving systems.

Challenge C1: Optimizing Resource Allocation and Navigating Bottlenecks in LMM Inference. The diverse characteristics of image-text and text-only requests, combined with variable arrival patterns and requests’ input heterogeneity, make managing bottlenecks in LMM inference pipelines particularly challenging for maximizing throughput. Bottlenecks can shift dynamically during bursts or when heavy-tailed requests arrive. For instance, during image bursts, the image preprocessing and encoding stages in LMM inference often become bottlenecks due to their compute-intensive nature and higher sensitivity to batching, as detailed in Section 3.3. In contrast, the language model backend may retain sufficient capacity to handle additional requests. Conversely, when heavy-tailed text requests with large prefill lengths arrive, the language model becomes the bottleneck due to the compute-intensive nature of the prefill stage, while the image encoder may remain underutilized. In such cases, a naive and coarse-grained approach like monolithic deployment (Section 2.2) will be highly resource-inefficient, as it requires scaling the

entire LMM pipeline, even when the bottleneck remains localized to a specific component.

Challenge C2: Achieving High Resource Utilization. The LMM inference pipeline often creates significant resource imbalances and may lead to poor resource utilization. Profiling of the Llama3.2-90B image encoder (Figure 7d) reveals this imbalance clearly. While it saturates compute resources, it uses only 2.5% of memory capacity and just 20% of available memory bandwidth. To balance compute and memory usage, the other two stages of the LMM pipeline, prefill and decode, can be combined using prefill-chunking [1, 20]. However, we observe that image-text requests are typically accompanied by small text prompts (much smaller than LLM serving). This limits opportunities to fuse prefill and decode operations, resulting in decode-only batches that underutilize compute resources. These imbalances make achieving high resource utilization in LMM inference extremely challenging.

Implication: Stage-Specific Optimizations. Different stages of LMM pipelines, such as image preprocessing, encoding, and text generation (LLM prefill and decode), exhibit distinct optimization characteristics and resource utilization patterns (Section 3.3). The efficacy of performance optimization techniques, particularly batching policies, model parallelization strategies, and GPU frequency scaling policies, varies significantly across different LMM stages and model architectures. This observation motivates the need for fine-grained, stage-aware configuration management to maximize throughput while maintaining latency constraints, and co-location of stages where possible, to maximize resource efficiency

5.2 Implications on Scheduling and Routing

Similar to LLM serving, in LMM serving, a scheduler determines when to batch or execute every request within each model instance, while a router distributes incoming requests across model instances to balance the load. The production traces (Section 4) exhibit highly variable and heterogeneous characteristics and pose several challenges to efficiently scheduling and routing LMM requests at scale.

Challenge C3: Managing Tail Latencies during Traffic Bursts. The bursts observed in production traces (Figure 14) can significantly increase queuing delays and lead to SLO violations. This is because the SLOs for LMM serving systems are defined on tail TTFT and TBT latencies (e.g., the P95 or P99), and these tail latencies (especially TTFT) remain highly sensitive to queuing. When the bursts happen, queuing is inevitable. LMMs complicate this as different modalities (such as image-text and text-only requests) can experience independent bursts, each imposing varying computational demands on the pipeline. Furthermore, reactive approaches may fail to address these issues effectively because bursts can cause SLO violations before the system has a chance to adapt.

Challenge C4: Handling Convoy Effects and Interference

from Heavy-Tailed Requests. The heavy-tailed and wide distribution of requests in terms of prompt lengths and image counts in production LMM traces, along with their distinct processing requirements, can cause convoy effects and increase performance interference. For example, a convoy effect may occur when text-only requests with long prompts occupy all the workers in the shared LMM inference cluster. This scenario can block image-text requests that are collocated with the text-only requests, even when the queues are short, increase their tail latency, and violate SLOs. Overall, a few large requests from one modality may increase the latency of many small requests from another modality, leading to SLO violations. To make things worse, the distinct processing requirements of image-text and text-only requests can further increase interference. For instance, as the percentage of image tokens increases in the context, prefill time decreases because image tokens bypass the self-attention layers in CA-based LMMs. However, since images can have varying token counts (from 256 to 8K tokens as shown in Figure 3), naively prioritizing image-text requests can degrade performance for text-only requests.

Implication: Modality-Aware Routing and Scheduling. Concurrent execution of text-only and image-text requests on shared LMM instances improves utilization but leads to significant performance variation (Section 3.4) that is mainly due to their distinct processing requirements and varying context lengths. For instance, request TTFT decreases when the percentage of image tokens in the total context length increases since image tokens bypass the self-attention layers (which accounts for a dominant portion of 32 out of 40 layers in Llama3.2-11B) in CA-based LMMs. However, since images can consist of a varying number of image tokens (ranging from 256 to up to 8K tokens as shown in Figure 3), simply prioritizing incoming image-text requests can lead to performance degradation for text-only requests.

To serve traffic bursts and minimize interference and convoy effects, modality-aware request routing and scheduling are essential. This approach should intelligently collocate text-only and image-text requests based on the token ratios of image and text in the request context, ensuring high resource utilization on shared GPU devices while meeting SLOs.

6 A Decoupled System Design

To address these challenges (Section 5), we present a *decoupled serving architecture* for LMM inference that **logically** splits operations into image- and text-specific nodes.

While this decoupled design effectively addresses resource allocation and dynamic inference bottleneck challenges outlined in C1 and C2 (Section 5.1), it also forms the building block for **modality-aware** scheduling and routing to address the issues of tail latency, heterogeneous request bursts, and interference highlighted in C3 and C4 (Section 5.2).

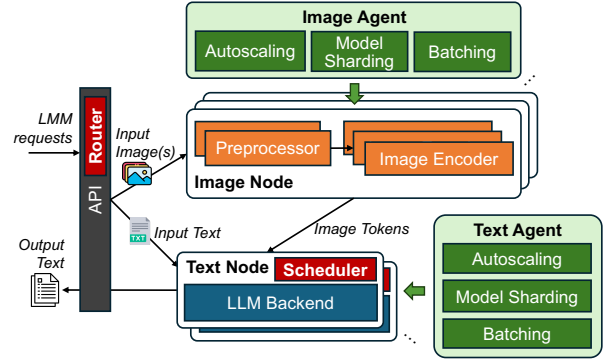


Figure 17: A decoupled design for LMM serving.

6.1 A Decoupled Architecture

Our comprehensive analysis reveals that the monolithic serving infrastructure for LMMs is inefficient; it neither caters to the diverse resource requirements of each stage of LMM inference nor optimizes the execution of these stages. We posit that logically separating the stages and independently optimizing their deployment improves serving efficiency.

Figure 17 illustrates this decoupled architecture. The *Image Nodes* process input images from the LMM requests, and each image node comprises one or more image preprocessors and image encoders from an LMM pipeline. Image tokens from Image Nodes are then sent to the *Text Nodes* for further text-based processing (*i.e.*, LLM prefill and decode) to generate the output text. Text-only requests can bypass the image-specific components and be queued directly at the Text Nodes. This approach minimizes interference in text-only requests, preventing resource contention caused by the encoder handling image-text requests.

This architectural separation provides three key benefits:

- This approach enables adaptive and independent resource scaling based on LMM workload characteristics, with Image Nodes handling image-specific operations such as pre-processing and encoding, and Text Nodes hosting the LLM backend that manages prefill and decode stages.
- The decoupled design allows stage-specific and model-specific configurations (*e.g.*, autoscaling, model parallelism, and batching strategies), optimized for each component’s computational profile and architecture.
- Cross-request interference can be minimized by physically separating Image and Text Nodes in this design, allowing text-only requests to bypass the Image Node entirely. In addition, modality-aware scheduling at the Text Node can maximize the processing throughput of text and image tokens while meeting the TTFT and TBT SLOs.

6.2 Decoupled Resource Management

The logical split between Image and Text Nodes allows for independent provisioning and management of the image-

specific and text-specific components in an LMM pipeline, each with varied resource demands. Our design introduces an *Image Agent* and *Text Agent* to independently manage resources and configurations for their respective components. Each agent dynamically makes online resource configuration decisions based on workload demands and system load. Below, we highlight three key features of decoupled resource management for LMM components.

- **Autoscaling.** The Image and Text Agents dynamically determine the number of replicas for each model component based on real-time workload demands. For instance, during high image traffic in image-heavy scenarios, the Image Agent scales up the number of replicas of the image preprocessor and encoder to keep up with the rate of text processing and minimize overall request latency. The Text Agent can dynamically adjust the number of replicas of the language model backend to manage prompt length spikes in prefill or decode operations. Depending on the deployment strategy, the language model prefill and decode can either be co-located [1, 20] or disaggregated [40, 56], and scaled accordingly to optimize performance.
- **Batching.** The Image and Text Agents independently decide whether incoming requests should be batched together to improve throughput or processed immediately to meet latency SLOs. For example, Image Nodes may avoid batching multiple image encoding requests to ensure low encoding latency if encoding is the bottleneck and GPU compute utilization is saturated, which oftentimes is achieved with very small batch sizes as shown in Section 3.3. Conversely, Text Nodes may batch requests to optimize token processing/generation throughput during the LLM’s prefill/decode stage, depending on the TTFT/TBT SLOs, especially for CA-based LMMs.
- **Model Sharding.** The agents configure optimal parallelism (TP/PP) degrees for their respective model components (image encoder and language model backend). Our experiments show that encoders generally achieve maximum throughput with a smaller TP compared to the LLM backend (Section 3.3). This independent model sharding is effectively enabled within our decoupled architecture.

6.3 Disaggregated Deployment

While our decoupled design logically separates an LMM serving system into Image and Text Nodes, a straightforward deployment strategy is to run these components on physically disaggregated GPUs; a one-to-one mapping between logical Image and Text Nodes to physical GPU nodes. Such a disaggregated deployment is latency-centric; physically separating the Image and Text Nodes minimizes interference between different types of requests, makes independent scaling decisions easier to deploy compared to a monolith architecture, and thus greatly reduces operational complexity. Disaggregation is especially useful when the multimodal workload is

highly dynamic, and each modality can exhibit independent bursts and heavy skews.

In addition, disaggregated deployment enables more effective utilization of heterogeneous hardware and independent GPU frequency scaling, optimizing both performance and energy efficiency. For instance, operators can allocate high-performance GPUs like H100 for image encoding and LLM prefill while older generations of GPUs for LLM decode [40].

6.4 Image-Encode-Text-Decode Colocation

One key challenge with the disaggregated deployment is that it can lead to suboptimal resource efficiency. As outlined in C2, the Image Nodes hosting the encoder are compute-heavy and gravely under-utilize memory capacity and bandwidth. While deploying encoders on a heterogeneous set of commodity GPUs might seem attractive, such a strategy would compromise latency guarantees required in production environments. Text Nodes, on the other hand, under-utilize both CPU (unlike Image Nodes that include CPU-intensive image preprocessing) and GPU compute due to limited opportunity to fuse prefill and decode operations.

To address this inefficiency, we propose *stage colocation*. The idea is to physically co-locate the LLM decode operations with image encoding on the same GPU instance, motivated by their opposite resource demand. The co-location strategy, however, introduces non-trivial technical challenges. First, the key-value cache has to be transferred from the Text Nodes to the Image Nodes. However, since this transfer happens only once (after the prefill phase), it can be overlapped with decode computation, resulting in minimal overhead in high-bandwidth clusters [40, 56]. Second, traditional GPU sharing mechanisms such as MPS [38] and MIG [37] can lead to unpredictable performance interference between the two interleaving stages. Selective operator fusion [6, 19] across stages can be investigated as a promising direction to achieve both predictable latency and improved throughput. However, this approach requires careful consideration of operation dependencies and resource constraints.

6.5 Modality-Aware Scheduling and Routing

Our decoupled architecture has an added advantage. By design, it enables routing and scheduling decisions that are aware of multimodal inputs. This improves system efficiency and addresses challenges C3 and C4 in the following manner.

Modality-Aware Routing. To address challenge C3, the routing techniques need to minimize the queuing delays that impact TTFT tail latency (Section 5.2). However, image bursts seen in the production traces (Section 4) make the routing techniques vulnerable to load imbalances, increasing queuing delays. Common LLM routing techniques, such as round-robin and memory-based load balancing [48], fail to mitigate this issue. Round-robin is unaware of request sizes and

can assign requests to model instances where small requests with few images get queued behind large ones with many images. Memory-based load balancing also falls short, as it fails to capture the computational load imposed by the compute-bound nature of image encoding (Section 3.3). We propose a modality-aware routing strategy that considers input modality to route requests to multiple Image Nodes with the least image tokens in the queue. This approach is effective because: (1) image tokens inherently reflect the number of images per request and image sizes, (2) image encoding is compute-bound, and (3) image processing loads are balanced across multiple preprocessors and encoders created by the Image Agent autoscaler. By parallelizing image token generation and prioritizing Image Nodes with the lowest image-token load, our proposed routing technique reduces queuing delays caused by image bursts, improving TTFT tail latency.

Modality-Aware Scheduling. To tackle challenge C4, scheduling techniques must handle convoy effects and interference between image-text and text-only requests. While disaggregated deployment (Section 6.3) naturally mitigates interference—preventing large image-text requests from blocking small text-only requests by confining them to Image Nodes—interference can still occur on Text Nodes. This happens when large text-only requests block image-text requests, as image-text requests require their text prefill to be processed on Text Nodes. Traditional scheduling techniques like FIFO fail to address this issue due to head-of-line blocking [41].

To prevent convoy effects and interference, our scheduling technique prioritizes requests based on both modality and prompt size, and mixes batched requests based on performance variation profiles with varying modality mixture for DO and CA models (Section 3.4). The key idea of our proposed technique is to give high priority to image-text requests and low priority to large-size text-only requests in the Text Nodes. Additionally, this prioritization scheme also allows preempting large text-only requests and rescheduling them to accommodate image-text requests, avoiding convoy effects and providing performance isolation in TTFT and TBT.

7 Related Work

LMM Characterization. Lee *et al.* [21] provides a comprehensive characterization of multimodal generation models at Meta, while we focus on multimodal inputs. Hou *et al.* [15] focus on traditional multimodal models employing small-scale convolutional neural networks. In contrast, our work presents a detailed analysis of multimodal input workloads on both open-source LMM models and production traces, highlighting their unique execution and workload patterns.

LMM Serving. Recent research has introduced several techniques to optimize LMM serving by addressing key inefficiencies in inference computation and memory usage. Inf-MLLM [35] employs token caching strategies and at-

tention bias to maintain performance with long contexts while reducing KV cache memory consumption. Elastic Cache [29] utilizes an importance-driven cache merging strategy to prune KV caches efficiently during inference. Dynamic-LLaVA [17], VTW [27], and QueCC [24] present various vision token sparsification and compression techniques to dynamically reduce redundancy in vision tokens. These optimizations primarily operate at the model level, trading off computational overhead with model performance. They are orthogonal to our proposed system-level design for SLO-driven LMM serving that does not impact model performance, which can further benefit from such model-level advancements, e.g., faster image encoding through token compression.

LLM Serving. Recent studies have delved into optimization for text-only LLM serving. For instance, DynamoLLM [47] enhances LLM serving efficiency through model parallelism, autoscaling, and frequency scaling. POLCA [39] introduces a framework for managing resource oversubscription in LLM inference clusters. Other optimizations for LLM serving include key-value cache management [20], continuous batching [54], scheduling [41–43, 46, 48], prefill-decode interference reduction [1, 40, 56]. While these optimizations enhance prefill and decode efficiency, our work focuses on the unique characteristics of multimodal models.

8 Conclusion

In this paper, we present a comprehensive systems analysis on LMM inference workloads through extensive benchmarking on open-source LMMs and production traces. Our characterization revealed unique challenges, including heterogeneous performance, resource, and power characteristics of various LMM components and performance interferences between multimodal requests. These insights led to our proposed decoupled architecture and systems design implications, such as modality-aware scheduling strategies, aimed at minimizing LMM serving cost and ensuring efficient LMM serving at scale. Our findings open up new avenues for future systems research on scalable, cost-efficient systems that address the complexities of multimodal inputs and LMM architectures.

References

- [1] Amey Agrawal, Nitin Kedia, Ashish Panwar, Jayashree Mohan, Nipun Kwatra, Bhargav Gulavani, Alexey Tumanov, and Ramachandran Ramjee. Taming Throughput-Latency Tradeoff in LLM Inference with Sarathi-Serve. In *Proceedings of the 18th USENIX Symposium on Operating Systems Design and Implementation (OSDI 2024)*, 2024.
- [2] Jean-Baptiste Alayrac, Jeff Donahue, Pauline Luc, Antoine Miech, Iain Barr, Yana Hasson, Karel Lenc, Arthur

- Mensch, Katherine Millican, Malcolm Reynolds, et al. Flamingo: a visual language model for few-shot learning. *2024 Conference on Neural Information Processing Systems (NeurIPS 2024)*, 35:23716–23736, 2022.
- [3] Dosovitskiy Alexey. An image is worth 16x16 words: Transformers for image recognition at scale. *arXiv preprint arXiv: 2010.11929*, 2020.
- [4] Reza Yazdani Aminabadi, Samyam Rajbhandari, Ammar Ahmad Awan, Cheng Li, Du Li, Elton Zheng, Olatunji Ruwase, Shaden Smith, Minjia Zhang, Jeff Rasley, et al. DeepSpeed-inference: Enabling efficient inference of transformer models at unprecedented scale. In *Proceedings of the 2022 International Conference for High Performance Computing, Networking, Storage and Analysis (SC 2022)*, pages 1–15. IEEE, 2022.
- [5] Jun Chen, Han Guo, Kai Yi, Boyang Li, and Mohamed Elhoseiny. VisualGPT: Data-efficient adaptation of pre-trained language models for image captioning. In *Proceedings of the 2022 IEEE/CVF Conference on Computer Vision and Pattern Recognition (CVPR 2022)*, pages 18030–18040, 2022.
- [6] Tianqi Chen, Thierry Moreau, Ziheng Jiang, Lianmin Zheng, Eddie Yan, Meghan Cowan, Haichen Shen, Leyuan Wang, Yuwei Hu, Luis Ceze, Carlos Guestrin, and Arvind Krishnamurthy. TVM: An automated end-to-end optimizing compiler for deep learning. In *Proceedings of the 13th USENIX Conference on Operating Systems Design and Implementation (OSDI 2018)*, page 579–594, USA, 2018. USENIX Association.
- [7] Xiaokang Chen, Zhiyu Wu, Xingchao Liu, Zizheng Pan, Wen Liu, Zhenda Xie, Xingkai Yu, and Chong Ruan. Janus-Pro: Unified multimodal understanding and generation with data and model scaling, 2025.
- [8] Zhe Chen, Weiyun Wang, Hao Tian, Shenglong Ye, Zhangwei Gao, Erfei Cui, Wenwen Tong, Kongzhi Hu, Jiapeng Luo, Zheng Ma, et al. How far are we to GPT-4V? Closing the gap to commercial multimodal models with open-source suites. *arXiv preprint arXiv:2404.16821*, 2024.
- [9] Zhe Chen, Jiannan Wu, Wenhai Wang, Weijie Su, Guo Chen, Sen Xing, Muyan Zhong, Qinglong Zhang, Xizhou Zhu, Lewei Lu, et al. InternVL: Scaling up vision foundation models and aligning for generic visual-linguistic tasks. In *Proceedings of the 2024 IEEE/CVF Conference on Computer Vision and Pattern Recognition (CVPR 2024)*, pages 24185–24198, 2024.
- [10] Chen, Zhe and Wu, Jiannan and Wang, Wenhai and Su, Weijie and Chen, Guo and Xing, Sen and Zhong, Muyan and Zhang, Qinglong and Zhu, Xizhou and Lu, Lewei and others. HuggingFace Model: OpenGVLab/InternVL2_5-26B. https://huggingface.co/OpenGVLab/InternVL2_5-26B, 2024.
- [11] Jianfeng Chi, Ujjwal Karn, Hongyuan Zhan, Eric Smith, Javier Rando, Yiming Zhang, Kate Plawiak, Zacharie Delpierre Coudert, Kartikeya Upasani, and Mahesh Pasupuleti. Llama Guard 3 Vision: Safeguarding human-AI image understanding conversations. *arXiv preprint arXiv:2411.10414*, 2024.
- [12] Wenliang Dai, Nayeon Lee, Boxin Wang, Zhuolin Yang, Zihan Liu, Jon Barker, Tuomas Rintamaki, Mohammad Shoeybi, Bryan Catanzaro, and Wei Ping. NVLM: Open Frontier-Class Multimodal LLMs, 2024.
- [13] Dai, Wenliang and Lee, Nayeon and Wang, Boxin and Yang, Zhuolin and Liu, Zihan and Barker, Jon and Rintamaki, Tuomas and Shoeybi, Mohammad and Catanzaro, Bryan and Ping, Wei. HuggingFace Model: nvidia/NVLM-D-72B. <https://huggingface.co/nvidia/NVLM-D-72B>, 2024.
- [14] Haodong Duan, Junming Yang, Yuxuan Qiao, Xinyu Fang, Lin Chen, Yuan Liu, Xiaoyi Dong, Yuhang Zang, Pan Zhang, Jiaqi Wang, et al. VLMEvalKit: An open-source toolkit for evaluating large multi-modality models. In *Proceedings of the 32nd ACM International Conference on Multimedia*, pages 11198–11201, 2024.
- [15] Xiaofeng Hou, Cheng Xu, Jiacheng Liu, Xuehan Tang, Lingyu Sun, Chao Li, and Kwang-Ting Cheng. Characterizing and understanding end-to-end multi-modal neural networks on GPUs. *IEEE Computer Architecture Letters*, 21(2):125–128, 2022.
- [16] Yushi Hu, Hang Hua, Zhengyuan Yang, Weijia Shi, Noah A Smith, and Jiebo Luo. PromptCap: Prompt-guided image captioning for VQA with GPT-3. In *Proceedings of the 2023 IEEE/CVF International Conference on Computer Vision (ICCV 2023)*, pages 2963–2975, 2023.
- [17] Wenxuan Huang, Zijie Zhai, Yunhang Shen, Shaoshen Cao, Fei Zhao, Xiangfeng Xu, Zheyu Ye, and Shaohui Lin. Dynamic-LLaVA: Efficient multimodal large language models via dynamic vision-language context sparsification. *arXiv preprint arXiv:2412.00876*, 2024.
- [18] HuggingFace. Image-Text-to-Text Models. https://huggingface.co/models?pipeline_tag=image-text-to-text&sort=trending, 2024.
- [19] Aditya K Kamath, Ramya Prabhu, Jayashree Mohan, Simon Peter, Ramachandran Ramjee, and Ashish Panwar. Pod-attention: Unlocking full prefill-decode overlap for

- faster LLM inference. *arXiv preprint arXiv:2410.18038*, 2024.
- [20] Woosuk Kwon, Zhuohan Li, Siyuan Zhuang, Ying Sheng, Lianmin Zheng, Cody Hao Yu, Joseph E. Gonzalez, Hao Zhang, and Ion Stoica. Efficient Memory Management for Large Language Model Serving with PagedAttention. In *Proceedings of the Symposium on Operating Systems Principles (SOSP 2023)*, 2023.
- [21] Yejin Lee, Anna Sun, Basil Hosmer, Bilge Acun, Can Balioglu, Changhan Wang, Charles David Hernandez, Christian Puhersch, Daniel Haziza, Driss Guessous, et al. Characterizing and efficiently accelerating multimodal generation model inference. *arXiv preprint arXiv:2410.00215*, 2024.
- [22] Bo Li, Yuanhan Zhang, Dong Guo, Renrui Zhang, Feng Li, Hao Zhang, Kaichen Zhang, Yanwei Li, Ziwei Liu, and Chunyuan Li. LLaVA-OneVision: Easy visual task transfer. *arXiv preprint arXiv:2408.03326*, 2024.
- [23] Bo Li, Yuanhan Zhang, Dong Guo, Renrui Zhang, Feng Li, Hao Zhang, Kaichen Zhang, Peiyuan Zhang, Yanwei Li, Ziwei Liu, and Chunyuan Li. LLaVA-OneVision: Easy Visual Task Transfer, 2024.
- [24] Kevin Y Li, Sachin Goyal, Joao D Semedo, and J Zico Kolter. Inference optimal VLMs need only one visual token but larger models. *arXiv preprint arXiv:2411.03312*, 2024.
- [25] Li, Bo and Zhang, Yuanhan and Guo, Dong and Zhang, Renrui and Li, Feng and Zhang, Hao and Zhang, Kaichen and Li, Yanwei and Liu, Ziwei and Li, Chunyuan. HuggingFace Model: Imms-lab/llava-onevision-qwen2-72b-ov-sft. <https://huggingface.co/Imms-lab/llava-onevision-qwen2-72b-ov-sft>, 2024.
- [26] Li, Bo and Zhang, Yuanhan and Guo, Dong and Zhang, Renrui and Li, Feng and Zhang, Hao and Zhang, Kaichen and Li, Yanwei and Liu, Ziwei and Li, Chunyuan. HuggingFace Model: Imms-lab/llava-onevision-qwen2-7b-ov. <https://huggingface.co/Imms-lab/llava-onevision-qwen2-7b-ov>, 2024.
- [27] Zhihang Lin, Mingbao Lin, Luxi Lin, and Rongrong Ji. Boosting multimodal large language models with visual tokens withdrawal for rapid inference. *arXiv preprint arXiv:2405.05803*, 2024.
- [28] Yixin Liu, Kai Zhang, Yuan Li, Zhiling Yan, Chujie Gao, Ruoxi Chen, Zhengqing Yuan, Yue Huang, Hanchi Sun, Jianfeng Gao, et al. Sora: A review on background, technology, limitations, and opportunities of large vision models. *arXiv preprint arXiv:2402.17177*, 2024.
- [29] Zuyan Liu, Benlin Liu, Jiahui Wang, Yuhao Dong, Guangyi Chen, Yongming Rao, Ranjay Krishna, and Jiwen Lu. Efficient inference of vision instruction-following models with elastic cache. In *European Conference on Computer Vision (ECCV 2025)*, pages 54–69. Springer, 2025.
- [30] Meta AI. HuggingFace Model: meta-llama/Llama-3.2-11B-Vision-Instruct. <https://huggingface.co/meta-llama/Llama-3.2-11B-Vision-Instruct>, 2024.
- [31] Meta AI. HuggingFace Model: meta-llama/Llama-3.2-90B-Vision-Instruct. <https://huggingface.co/meta-llama/Llama-3.2-90B-Vision-Instruct>, 2024.
- [32] Microsoft Azure. Azure VM ND-H100-v5 sizes series. <https://learn.microsoft.com/en-us/azure/virtual-machines/sizes/gpu-accelerated/ndh100v5-series?tabs=sizebasic>, 2024.
- [33] Microsoft Azure. Azure VM NDm-A100-v4 sizes series. <https://learn.microsoft.com/en-us/azure/virtual-machines/sizes/gpu-accelerated/ndma100v4-series?tabs=sizebasic>, 2024.
- [34] Ron Mokady, Amir Hertz, and Amit H Bermano. Clip-Cap: CLIP prefix for image captioning. *arXiv preprint arXiv:2111.09734*, 2021.
- [35] Zhenyu Ning, Jieru Zhao, Qihao Jin, Wenchao Ding, and Minyi Guo. Inf-MLLM: Efficient streaming inference of multimodal large language models on a single GPU. *arXiv preprint arXiv:2409.09086*, 2024.
- [36] NVIDIA. NVIDIA DCGM: Manage and monitor GPUs in cluster environments. <https://developer.nvidia.com/dcgm>, 2024.
- [37] NVIDIA. NVIDIA multi-instance GPU (MIG). <https://www.nvidia.com/en-us/technologies/multi-instance-gpu/>, 2024.
- [38] NVIDIA. NVIDIA multi-process service. <https://docs.nvidia.com/deploy/mps/index.html>, 2024.
- [39] Pratyush Patel, Esha Choukse, Chaojie Zhang, Íñigo Goiri, Brijesh Warriar, Nithish Mahalingam, and Ricardo Bianchini. Characterizing Power Management Opportunities for LLMs in the Cloud. In *Proceedings of the 29th ACM International Conference on Architectural Support for Programming Languages and Operating Systems (ASPLOS 2024)*, 2024.
- [40] Pratyush Patel, Esha Choukse, Chaojie Zhang, Aashaka Shah, Íñigo Goiri, Saeed Maleki, and Ricardo Bianchini. Splitwise: Efficient generative LLM inference using

- phase splitting. In *Proceedings of the 2024 ACM/IEEE 51st Annual International Symposium on Computer Architecture (ISCA 2024)*, pages 118–132. IEEE, 2024.
- [41] Archit Patke, Dharmath Reddy, Saurabh Jha, Haoran Qiu, Christian Pinto, Chandra Narayanaswami, Zbigniew Kalbarczyk, and Ravishankar Iyer. Queue management for SLO-oriented large language model serving. In *Proceedings of the 2024 ACM Symposium on Cloud Computing (SoCC 2024)*, pages 18–35, 2024.
- [42] Haoran Qiu, Weichao Mao, Archit Patke, Shengkun Cui, Saurabh Jha, Chen Wang, Hubertus Franke, Zbigniew Kalbarczyk, Tamer Başar, and Ravishankar K. Iyer. Power-aware Deep Learning Model Serving with μ -Serve. In *USENIX Annual Technical Conference (USENIX ATC 2024)*, 2024.
- [43] Haoran Qiu, Weichao Mao, Archit Patke, Shengkun Cui, Saurabh Jha, Chen Wang, Hubertus Franke, Zbigniew T. Kalbarczyk, Tamer Başar, and Ravishankar K. Iyer. Efficient Interactive LLM Serving with Proxy Model-based Sequence Length Prediction. In *The 5th International Workshop on Cloud Intelligence / AIOps at ASPLOS 2024*, 2024.
- [44] Dustin Schwenk, Apoorv Khandelwal, Christopher Clark, Kenneth Marino, and Roozbeh Mottaghi. A-OKVQA: A benchmark for visual question answering using world knowledge. In *Proceedings of the 2022 European Conference on Computer Vision (ECCV 2022)*, pages 146–162. Springer, 2022.
- [45] Zhenwei Shao, Zhou Yu, Meng Wang, and Jun Yu. Prompting large language models with answer heuristics for knowledge-based visual question answering. In *Proceedings of the 2023 IEEE/CVF Conference on Computer Vision and Pattern Recognition (CVPR 2023)*, pages 14974–14983, 2023.
- [46] Jovan Stojkovic, Chaojie Zhang, Íñigo Goiri, Esha Choukse, Haoran Qiu, Rodrigo Fonseca, Josep Torrellas, and Ricardo Bianchini. TAPAS: Thermal-and power-aware scheduling for LLM inference in cloud platforms. *arXiv preprint arXiv:2501.02600*, 2025.
- [47] Jovan Stojkovic, Chaojie Zhang, Íñigo Goiri, Josep Torrellas, and Esha Choukse. DynamoLLM: Designing LLM Inference Clusters for Performance and Energy Efficiency. In *Proceedings of the IEEE International Symposium on High Performance Computer Architecture (HPCA 2025)*, 2025.
- [48] Biao Sun, Ziming Huang, Hanyu Zhao, Wencong Xiao, Xinyi Zhang, Yong Li, and Wei Lin. Llumnix: Dynamic scheduling for large language model serving. *arXiv preprint arXiv:2406.03243*, 2024.
- [49] Gemini Team, Petko Georgiev, Ving Ian Lei, Ryan Burnell, Libin Bai, Anmol Gulati, Garrett Tanzer, Damien Vincent, Zhufeng Pan, Shibo Wang, et al. Gemini 1.5: Unlocking multimodal understanding across millions of tokens of context. *arXiv preprint arXiv:2403.05530*, 2024.
- [50] vLLM. Distributed Inference and Serving. https://docs.vllm.ai/en/latest/serving/distributed_serving.html, 2024.
- [51] Guan Wang, Sijie Cheng, Xianyuan Zhan, Xiangang Li, Sen Song, and Yang Liu. OpenChat: Advancing open-source language models with mixed-quality data. *arXiv preprint arXiv:2309.11235*, 2023.
- [52] A Waswani, N Shazeer, N Parmar, J Uszkoreit, L Jones, A Gomez, L Kaiser, and I Polosukhin. Attention is all you need. In *2017 Conference on Neural Information Processing Systems (NIPS 2017)*, 2017.
- [53] Thomas Wolf, Lysandre Debut, Victor Sanh, Julien Chaumond, Clement Delangue, Anthony Moi, Pierric Cistac, Tim Rault, Rémi Louf, Morgan Funtowicz, Joe Davison, Sam Shleifer, Patrick von Platen, Clara Ma, Yacine Jernite, Julien Plu, Canwen Xu, Teven Le Scao, Sylvain Gugger, Mariama Drame, Quentin Lhoest, and Alexander M. Rush. Transformers: State-of-the-art natural language processing. In *Proceedings of the 2020 Conference on Empirical Methods in Natural Language Processing: System Demonstrations*, pages 38–45. Online, October 2020. Association for Computational Linguistics.
- [54] Gyeong-In Yu, Joo Seong Jeong, Geon-Woo Kim, Soojeong Kim, and Byung-Gon Chun. Orca: A Distributed Serving System for Transformer-Based Generative Models. In *Proceedings of the 16th USENIX Symposium on Operating Systems Design and Implementation (OSDI 2022)*, 2022.
- [55] Xiaohua Zhai, Basil Mustafa, Alexander Kolesnikov, and Lucas Beyer. Sigmoid Loss for Language Image Pre-Training. In *2023 IEEE/CVF International Conference on Computer Vision (ICCV 2023)*, pages 11941–11952, Paris, France, October 2023. IEEE.
- [56] Yinmin Zhong, Shengyu Liu, Junda Chen, Jianbo Hu, Yibo Zhu, Xuanzhe Liu, Xin Jin, and Hao Zhang. Dist-Serve: Disaggregating prefill and decoding for goodput-optimized large language model serving. In *Proceedings of the 18th USENIX Symposium on Operating Systems Design and Implementation (OSDI 2024)*, pages 193–210, 2024.